Interaction Potentials, Spectroscopy, and Transport Properties of the Br^+−RG Systems (RG = He−Ar)†

Alexei A. Buchachenko,*,‡ Timothy G. Wright,*,§ Edmond P. F. Lee,*,∥ and Larry A. Viehland*,⊥

Laboratory of Molecular Structure and Quantum Mechanics, Department of Chemistry, Moscow State Universty, Moscow 119991, Russia, School of Chemistry, University of Nottingham, University Park, Nottingham NG7 2RD, United Kingdom, School of Chemistry, University of Southampton, Highfield, Southampton SO17 1BJ, United Kingdom, and Department of Science, Chatham University, Pittsburgh, Pennsylvania 15232

Received: April 25, 2009; Revised Manuscript Received: June 24, 2009

The potential energy curves of Br cations interacting with rare gas (RG = He−Ar) atoms are calculated employing the RCCSD(T) technique for the non-spin−orbit states, with spin−orbit coupling being included analytically, using an atoms-in-molecule approach. The curves are calculated employing large basis sets extrapolated to the complete basis set limit, and the energies are corrected for basis set superposition error. Comparison is made to the limited potentials available previously. Gaseous ion mobilities are obtained using the potential energy curves of the states of the complex that correlate to the $Br^+(^3P_J°)$ + RG asymptotes. Excellent agreement is obtained with the experimental data in He; however, the experimental error bars are such that we are unable to determine which spin−orbit state(s) are present in the mobility measurements. Finally, a high-resolution photoelectron spectrum is simulated for the ionization of Br−Ar.

Introduction

Determination of interatomic forces from spectroscopic and transport properties is among the oldest tasks of physical chemistry and molecular physics.[1] Nevertheless, it still presents many challenges even for the simplest case of interactions with the rare gas atoms. On the one hand, advances in experimental techniques provide very precise data that are sensitive to specific features of the interactions. On the other, the limitations of the various methods do not allow them to probe the interaction potential energy function over wide ranges of internuclear distances, making it necessary to combine information from different sources. This dichotomy is especially true for open-shell atoms whose interactions with rare gases can be viewed as anisotropic;[2] i.e., they give rise to different molecular states that correlate to the same atomic multiplets. The splittings between them frequently are compounded by spin−orbit splitting, so that a complete description of the interatomic forces implies the construction of either the diabatic potential matrix or the set of adiabatic potentials. It is not always easy to extract all the parameters from experimental data. Involvement of ab initio theory helps a lot, but this introduces its own problems, associated primarily with accuracy issues.

Owing to extensive gas-phase transport measurements,[3−6] halogen anions, as well as alkali metal cations,[7−10] interacting with the rare gases (RG) have become paradigms for studying and understanding closed-shell ion−neutral interactions. Direct inversion of the potentials from transport coefficients[11,12] and the testing of various empirical and semiempirical potential models[13−18] and correlation relations[19,20] were accomplished in the 1980s and early 1990s. New information on interactions involving the halogen anions X^- and atoms X has come with the development of high-resolution photoelectron (zero electron kinetic energy, ZEKE) spectroscopy that allows the $X^-(^1S)$−RG interaction potential to be probed in the vicinity of the van der Waals minimum (see, e.g., refs 21−26). Although the spectroscopic potentials derived from ZEKE measurements appeared to be superior to the previous model potentials,[27−30] they still do not reproduce the measured ion mobilities within experimental error, most likely because of uncertainties in the spectroscopically inaccessible regions of the potentials.

Interest in interactions involving the open-shell $X(^2P)$ neutrals arose independently in the 1970s after the detection of UV emission[31−33] and laser action[34−36] of the excited excimer states. Most of the emission measurements, however, tell us little about the lowest electronic states and even modern high-resolution spectroscopy has characterized quantitatively only a few of the heaviest Xe complexes (see, e.g., ref 37 and references therein). More informative are the crossed molecular beam experiments pioneered by Lee and co-workers[38−41] and extended by the Perugia group (see, e.g., refs 42−44). In many cases the measurements of integral and differential scattering cross sections with magnetic selection of the initial state made it possible to probe the interactions in all states of the $X(^2P)$−RG manifold. High-quality information also has emerged from the above-mentioned ZEKE spectroscopy.[21−26] Both methods can be used to deduce empirical interaction potentials, but quite naturally, the scattering potentials appeared to be not very accurate for spectroscopic measurements and vice versa.[27,28] Limited measurements of neutral transport properties[45,46] and intramultiplet transition rate constants[47−51] are also available.

Progress in the experimental characterization of the X^-−RG and X−RG potentials was accompanied by rapid improvement

† Part of the "Vincenzo Aquilanti Festschrift".

* Corresponding authors: alexei@classic.chem.msu.su; tim.wright@nottingham.ac.uk; e.p.lee@soton.ac.uk; viehland@chatham.edu.

‡ Laboratory of Molecular Structure and Quantum Mechanics, Department of Chemistry, Moscow State Universty, Moscow 119991, Russia.

§ School of Chemistry, University of Nottingham, University Park, Nottingham NG7 2RD, United Kingdom.

∥ School of Chemistry, University of Southampton, Highfield, Southampton SO17 1BJ, United Kingdom.

⊥ Department of Science, Chatham University, Pittsburgh, Pennsylvania 15232, United States.

10.1021/jp903811b
Published on Web 07/15/2009

of the ab initio results. Early multiconfiguration calculations were oriented mostly toward the excimer electronic states (see, e.g., refs 52−55) and were unable to reproduce the polarization forces responsible for bonding in the lowest states. The single-reference perturbation approaches implemented with basis sets of triple and quadruple-ζ quality came as the first alternative.[56−59] Comparisons with the transport, scattering, and spectroscopic data revealed the need for using coupled cluster methods with the perturbative correction to triple excitations, CCSD(T). Basis sets of quadruple- and quintuple-ζ quality heavily augmented by diffuse and/or bond functions, as well as their extrapolation to the complete basis set limit, have been used to improve the description of the polarization forces, whereas for the heavier systems the ab initio treatment of the spin−orbit coupling has been tried.[27−30,60−64] The best potentials available presently for the neutral and anion complexes of chlorine, bromine, and iodine withstood rigorous multiproperty assessment against the existing experimental data. However, there is still some room to improve them: typical accuracy for transport and scattering data is around 5%; the error in ZEKE transition energies amounts typically to 10−20 cm^{-1} but in some cases approaches 40 cm^{-1}.[28−30,63,64]

In contrast, much less is known about the interactions involving the open-shell $X^+(^3P°)$ cations, among which only the I^+−RG systems with RG = He−Ar have been the subject of accurate ab initio study.[29] In the present paper we address the Br^+ complexes with the same partners, as a continuation of our previous studies on their negatively charged and neutral counterparts.[30,64] The successes of the previous studies to some extent justifies the accuracy of the present potentials and compensates for the lack of experimental data for direct comparison. Indeed, only the Br^+−He potential can be tested against the measured transport properties.[6,65,66]

Interaction Potentials

Scalar-Relativistic Potentials. Within the nonrelativistic or scalar-relativistic (SR) approximation, the ground term of the Br^+ cation has $^3P°$ symmetry. Interaction with an RG atom splits it into $^3\Sigma^-$ and $^3\Pi$ molecular states.[29] In what follows we will denote the potential energy curves of these states (as functions of internuclear distance, R) as V_Σ and V_Π, respectively.

These potentials were calculated ab initio with the MOLPRO program package[67] using the restricted version of the CCSD(T) method, or RCCSD(T). SR effects were taken into account by employing the ECP10MDF relativistic effective core potential (ECP) for the bromine cation.[68] The RG atoms were treated with all-electron basis sets. The augmented, correlation-consistent, polarized valence, $n\zeta$ aug-cc-pVnZ basis sets[68−70] were used for all centers, Br and RG, always extended by a further set of primitives of all angular momenta types, in an even-tempered way, based upon the ratio between the two most diffuse orbitals. This is essentially equivalent to the double augmentation to the cc-pVnZ set, and we denoted these basis sets DAVnZ.

Interaction energies were obtained for a wide range of R with basis sets of quadruple-ζ (n = Q, DAVQZ) and quintuple-ζ (n = 5, DAV5Z) quality, corrected for basis set superposition error by applying the full counterpoise correction[71] and extrapolated, at each R, to the complete basis set (CBS) limit employing the two-point extrapolation formulas of Helgaker and co-workers.[72,73] Note that exactly the same approach was followed in our previous study of the Br^-−RG and Br−RG interactions.[64]

To verify the quality of these calculations, we used the finite-field approximation to compute the static dipole polarizabilities of the atoms and ions involved. Those for RG atoms have already been presented in ref 64 and agree with accurate data to within 0.01 a_0^3, whereas those for Br ions and neutrals are presented in Table 1 together with the most relevant literature values.[74−78] For the $Br^-(^1S)$ anion, the present polarizability value exceeds the empirical estimate by Coker,[74] often referred to as experimental, and the value deduced from the calculated photodetachment cross section,[75] but agrees well with the most accurate theoretical calculations by the time-dependent perturbation theory.[76] For $Br(^2P)$ and $Br^+(^3P°)$, there are two polarizability components, α_Σ and α_Π, that differ in the projection of the orbital electronic angular momentum onto the field axis. They can be converted to isotropic (scalar) and anisotropic (tensorial) polarizabilities using $\alpha_0 = (\alpha_\Sigma + 2\alpha_\Pi)/3$ and $\alpha_2 = (\alpha_\Pi - \alpha_\Sigma)/3$, respectively.[79] The best available theoretical estimates[77,78] support the accuracy of the present values—see Table 1.

TABLE 1: Comparison of the Static Dipole Polarizabilities of the Br Atom and Ions (a_0^3) Calculated Here at the RCCSD(T)/DAV5Z Level of Theory with the Literature Values

species	source	α_Σ	α_Π	α_0	α_2
$Br^-(^1S)$	ref 74	35 ± 1		35 ± 1	
	ref 75	42.51		42.51	
	ref 76	49.05		49.05	
	this work	48.42		48.42	
$Br(^2P)$	ref 77	18.90	22.01	20.97	1.04
	ref 78			21.76	0.67
	this work	19.17	21.81	20.93	0.88
$Br^+(^2P°)$	ref 77	13.01	11.89	12.26	−0.37
	this work	12.93	12.08	12.36	−0.28

TABLE 2: Parameters of the ab Initio SR Br^+−RG Potentials: R_e (Å), D_e (cm^{-1}), D_0 (cm^{-1}), D_6 (a.u.) and C_6 (a.u.)[a]

RG	Λ	basis	R_e	D_e	D_0	D_6	C_6
He	Σ	DAVQZ	3.456	79.5	53.4	6.0	4.8
		DAV5Z	3.445	80.9	54.5	5.7	4.3
		CBS	3.433	82.5	55.7	5.5	4.3
	Π	DAVQZ	2.956	185.9	140.8	15.9	14.7
		DAV5Z	2.945	190.2	144.3	15.6	14.4
		CBS	2.933	194.8	148.2	15.3	15.1
Ne	Σ	DAVQZ	3.454	161.8	141.8	14.6	10.9
		DAV5Z	3.446	164.0	143.8	14.0	10.3
		CBS	3.438	166.4	146.1	14.2	10.5
	Π	DAVQZ	2.973	376.3	342.7	33.9	30.2
		DAV5Z	2.962	382.8	348.8	33.1	29.7
		CBS	2.950	389.9	355.5	32.2	28.5
Ar	Σ	DAVQZ	3.684	473.5	449.0	52.7	25.6
		DAV5Z	3.669	486.2	461.1	50.7	23.6
		CBS	3.652	499.9	474.4	50	23
	Π	DAVQZ	2.851	1971.9	1909.6	134.7	107.6
		DAV5Z	2.838	2039.3	1975.9	132.6	105.5
		CBS	2.823	2112.6	2047.8	132	105

[a] The number of digits in D_6 and C_6 values reflects the accuracy of the fits.

Table 2 shows the equilibrium parameters of the SR potentials calculated using the DAVQZ and DAV5Z basis sets and extrapolated to the CBS limit: the equilibrium distance, R_e, the binding energy, D_e, obtained with a spline interpolation of the ab initio points, and the dissociation energy, D_0, computed by solving the Schrödinger equation numerically. (Note that spectroscopic properties reported here are for the most abundant isotopes, ^{79}Br, ^4He, ^{20}Ne, and ^{40}Ar.)

The Br^+−RG interaction is strongly anisotropic, as the ratio of binding energies in the two electronic states, $\beta_{\Sigma\Pi} = D_e(\Sigma)/D_e(\Pi)$, is about 2.3 for He and Ne and as large as 4.2 for Ar.

TABLE 3: Parameters of the Isotropic Interactions of the Br Cations, Neutrals, and Anions with RG, Obtained from the CBS-Extrapolated Potentials of the Present Paper and of Reference 64

RG	parameter	cation	neutral	anion
He	R_e, Å	3.14	3.86	4.09
	D_e, cm^{-1}	136	18	35
	C_6, a.u.	12	15	27
Ne	R_e, Å	3.15	3.78	3.96
	D_e, cm^{-1}	274	44	110
	C_6, a.u.	23	31	48
Ar	R_e, Å	3.13	3.95	3.87
	D_e, cm^{-1}	1130	119	446
	C_6, a.u.	78	110	174

This ratio is somewhat sensitive to the quality of the basis set, increasing slightly for Ar from 4.19 with the DAV5Z basis set to 4.23 upon the CBS extrapolation. The reason is that the Π-state interactions exhibit a slightly stronger dependence on basis set saturation. Extrapolation to the CBS limit recovers a further 1−3% of the bonding with respect to DAV5Z level, leading to a quite sizable gain of 70 cm^{-1} for D_e and D_0 in the case of Ar.

Table 2 also contains the long-range (LR) coefficients. The coefficients D_6 of the R^{-6} terms in the LR expansions were obtained by the fit to ab initio points at $R \geq 15$ Å after extraction of the lowest-order induction term $-D_4/R^4$, with $D_4 = \alpha_d(RG)/2$. The dispersion coefficient, C_6, is given by $D_6 = C_6 + \alpha_q(RG)/2$, where $\alpha_d(RG)$ and $\alpha_q(RG)$ are the static dipole and quadrupole polarizabilities of the RG atom.[13,64] The LR interactions are also strongly anisotropic, with the C_6 coefficient having opposite behavior to the Br^+ polarizabilities.

The anisotropy of the long-range forces, however, may not be strong enough to explain the large difference of the Σ- and Π-state bonding. Formation of the Σ^- state implies the $p_x^1p_y^1p_z^2$ electronic configuration of the Br^+ ion, in which the doubly occupied orbital points toward the Ar atom aligned along the z-axis. For the Π-state, $p_x^1p_y^2p_z^1$ or $p_x^2p_y^1p_z^1$ electronic configurations are required, in which a single electron occupies the orbital in Ar direction. It creates a more favorable condition for incipient chemical bonding. A contribution of this type is likely responsible for the bond length contraction in $Br^+-Ar(^3\Pi)$ with respect to the $Br^+-Ne(^3\Pi)$ cation. Note that the bond length in the $^3\Sigma^-$ state increases from He to Ar in accord with increasing van der Waals radius, as expected for typical interaction between closed-shell species.

The present results for the cationic complexes can be compared with our previous data on their neutral and negatively charged counterparts, obtained at the same level of ab initio theory.[64] In the case of a P-state atom or cation it is convenient to use the isotropic interaction potential defined as[2]

$$V_0 = (V_\Sigma + 2V_\Pi)/3 \quad (1)$$

In Table 3 we compare the equilibrium and LR parameters of the V_0 potentials for the $Br^{0,\pm}$ complexes with He, Ne, and Ar. The dispersion contributions to the binding energies increase from the cation to the neutral and then to the anion, in line with increasing polarizability. Much more important, however, is the effect of increasing exchange repulsion seen in the elongation of the equilibrium distance along the same sequence. As a result, induction and incipient chemical bonding make the cations much more strongly bound than the anions.

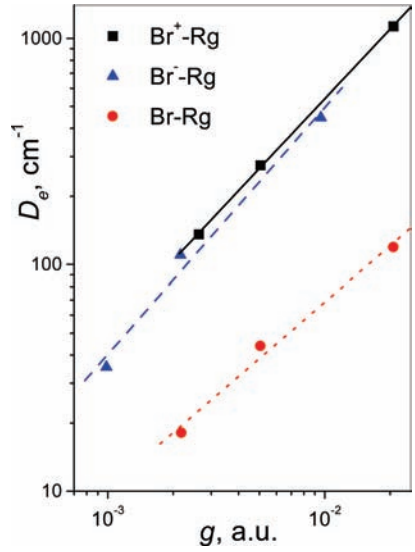

Figure 1. Correlation between the binding energies and g_{neutr} and g_{ion} functions for interactions of the Br atom and ions with RG from He to Ar (g increases accordingly). To represent neutrals on the same scale, g_{neutr} was multiplied by 10^{-4}.

These qualitative remarks find support in the useful correlation rules developed and analyzed by the Perugia group.[80−82] For the neutrals, the binding energy is assumed to be proportional to the lowest-order dispersion term

$$D_e \propto \frac{C_6}{R_e^6} = g_{neutr} \quad (2)$$

while for the ions it is proportional to the lowest-order induction term

$$D_e \propto \frac{\alpha_d(RG)}{R_e^4}(1 + \rho) = g_{ion} \quad (3)$$

where the parameter

$$\rho = \frac{C_6}{D_4 R_e^2} \quad (4)$$

accounts for the dispersion contributions. In Figure 1, the data of Table 3 are presented with g, D_e coordinates (in cm^{-1} and Å units). It is evident that the above correlations hold very well. The proportionality coefficient for neutrals is 0.76, slightly above the "universal" factor 0.72 from ref 81. The coefficients for the cations and anions are 5.5×10^4 and 4.6×10^4, respectively. Note that the value established[82] for Li^+-RG interactions is 4.2×10^4.

Vectorial Spin−Orbit Coupling. The electronic structure of the halogen cations is not complete without consideration of the vectorial spin−orbit (SO) coupling. It splits the ground $^3P^\circ$ term into three $^3P_J^\circ$ components with the total electronic angular momentum J equal to 2, 1, and 0. The excitation energies of the $J = 1$ and $J = 0$ components, relative to the ground $J = 2$ component, are $\Delta_1 = 3136.4$ and $\Delta_0 = 3837.5$ cm^{-1}, respectively.[83]

Interaction of the three $^3P_J°$ states of Br^+ with RG leads to six SO-coupled molecular adiabatic states. They can be classified using the conventional Hund case (c) notation as $n\Omega^\sigma$, where n is the term symbol, Ω is the projection of J onto the internuclear axis, and σ is the inversion parity. An alternative classification ($J\Omega$) emphasizes the connection to the atomic total electronic angular momentum J value, which is a good quantum number in the separated atom limit. Therefore, the three states $X^+2(22)$, $I^+1(21)$, and $I^+0^+(20)$ correlate to the $^3P_2°$ ground term of the cation, the two states $II^+1(11)$ and $II^+0^-(10)$ correlate to the $^3P_1°$ term and the $III^+0^+(00)$ state correlates to the $^3P_0°$ term. In what follows, we will omit σ and the ($J\Omega$) indices for simplicity.

The structure of the Br^+ multiplet indicates that these states cannot be considered as isolated. Indeed, the simplest approximation (valid for an isolated multiplet) to the SO operator

$$\hat{V}_{SO} = a\hat{L}\cdot\hat{S} \tag{5}$$

(a is the SO constant, while $\hat{L}$ and $\hat{S}$ are the total electronic orbital and spin angular momentum operators) predicts that the ratio of SO splittings, Δ_0/Δ_1, should be equal to 1.5. In contrast, the real ratio is much smaller, 1.224. Interactions with higher molecular states, such as those correlating to the excited $Br^+(^1D) + RG(^1S)$ limit, are expected to be important. To investigate these, we performed state-interacting SO calculations on Br^+-He including the states which correlate to both $^3P°$ and ^1D terms, namely, $^3\Sigma^-$, $^3\Pi$, $^1\Delta$, $^1\Sigma^+$, and $^1\Pi$, to describe the 14 lowest SO-coupled states.

In these calculations, we used the ECP10MDF spin−orbit effective core potential for Br^+, with the associated AVQZ valence basis set,[84] and the AVQZ basis set for He. The nonperturbed SR energies were obtained by the internally contracted multireference configuration interaction method (including the Davidson correction, Q), whereas the spin−orbit matrix elements were computed on the state-averaged complete active space self-consistent field wave functions.[85] In the limit of separated atoms, we obtained SO splittings Δ_1 and Δ_0 of 2699 and 4114 cm^{-1}, respectively, when only considering the nine SO states which arise from the $Br^+(^3P°) + He$ asymptote. Their ratio, 1.52, is almost identical to what should be expected for isolated multiplet. When all 14 SO states were considered, the asymptotic states lose some of the desired degeneracy but give improved splittings of 3250 and 3990 cm^{-1}; the ratio of 1.23 is in excellent agreement with experiment.

These calculations suggest that even more states than those employed herein are required for the state-interacting SO treatment in order to obtain the correct asymptotic SO atomic splittings. In addition, as RG gets heavier, charge transfer may come into play. This will lead to the involvement of states corresponding to the $Br(^2P) + RG^+(^2P)$ limit, such as has been found in the case of Br^+-Kr.[86] The extensive multireference and SO calculations for rapidly increasing number of molecular states will become progressively more demanding and limit the accuracy of the treatment of any individual state. Improvement of the intermultiplet splitting would therefore cause the loss of accuracy for the SR states arising from the lowest $^3P°$ asymptote.

As a compromise, we choose to account for the vectorial SO coupling via the standard atoms-in-molecule model for the ^3P_J multiplet (see, e.g., refs 2, 29, 87−89 and references therein) based on eq 5 but parametrized with the measured SO splittings. It leads to the well-known expressions for SO-coupled interaction potentials

$$V_{X+2} = V_\Pi$$

$$V_{I+1} = \frac{1}{2}(V_\Sigma + V_\Pi + \Delta_1 - \delta_1)$$

$$V_{I+0} = \frac{1}{2}(V_\Sigma + V_\Pi + \Delta_0 - \delta_0)$$

$$V_{II+1} = \frac{1}{2}(V_\Sigma + V_\Pi + \Delta_1 + \delta_1)$$

$$V_{II+0} = V_\Pi + \Delta_1$$

$$V_{III+0} = \frac{1}{2}(V_\Sigma + V_\Pi + \Delta_0 + \delta_0) \tag{6}$$

where $\delta_1^2 = (V_\Sigma - V_\Pi)^2 + \Delta_1^2$ and $\delta_0^2 = (V_\Sigma - V_\Pi)^2 - (2/3)\Delta_0(V_\Sigma - V_\Pi) + \Delta_0^2$. These expressions empirically take into account the intramultiplet SO coupling in the atomic ion but not its variation due to interaction with RG. Our previous experience for the Br−RG systems indicates that deviations from such behavior become noticeable in the complexes of Kr and Xe.[64] This is one of the reasons why we limited ourselves here to the lighter rare gases, from He to Ar.

The SO-coupled potentials computed using eq 6 and the V_Σ and V_Π functions of the CBS level of ab initio theory are characterized in Table 4. In addition to equilibrium properties and excitation energies, we present rotational and vibrational constants obtained by fitting the calculated energy levels. Note that the vibrational constants, ω_e and $\omega_e x_e$, are not good representations of the shallow and very anharmonic Br^+-He potential.

Ion Mobilities. To calculate the mobility of gaseous Br^+ ions in the rare gases, we used a standard approach[91,90] in which the total transport cross sections are obtained as the weighted sum of those for the individual SO-coupled potentials. The individual cross sections were calculated with the classical-mechanical program QVALUES[93,94] from the CBS potentials.

TABLE 4: Parameters of the SO-Coupled Br^+-RG Interactions (cm^{-1} unless otherwise stated)

state	T_e	R_e, Å	D_e	D_0	B_0	ω_e	$\omega_e x_e$	ω_{01}
				He				
X^+2	0	2.933	194.8	148.2	0.478	93	12.1	70.8
I^+1	77	3.218	118.3	84.7	0.391	64	9.3	47.0
I^+0	91	3.297	103.6	72.6	0.370	57	8.5	41.0
II^+0	3136	2.933	194.8	148.2	0.478	93	12.1	70.8
II^+1	3214	3.233	116.9	82.9	0.386	63	9.3	46.6
III^+0	3897	3.149	135.0	97.7	0.409	71	10.1	52.6
				Ne				
X^+2	0	2.950	389.9	355.5	0.119	67.0	3.11	62.8
I^+1	149	3.215	240.5	215.5	0.099	47.0	2.46	44.7
I^+0	180	3.297	210.0	186.8	0.094	43.7	2.47	41.0
II^+0	3136	2.950	389.9	355.5	0.119	67.0	3.11	62.8
II^+1	3292	3.244	234.5	209.1	0.097	47.9	2.66	44.9
III^+0	3957	3.162	270.7	242.9	0.103	53.2	2.84	49.6
				Ar				
X^+2	0	2.823	2112.6	2047.8	0.079	128.5	2.21	124.2
I^+1	992	2.967	1120.9	1082.2	0.071	73.7	1.30	71.9
I^+0	1346	3.294	766.7	739.0	0.058	54.2	0.97	52.2
II^+0	3136	2.823	2112.6	2047.8	0.079	128.5	2.21	124.2
II^+1	4457	3.399	791.8	755.8	0.054	70.1	1.83	66.9
III^+0	4964	3.280	985.8	943.3	0.058	82.9	2.07	79.4

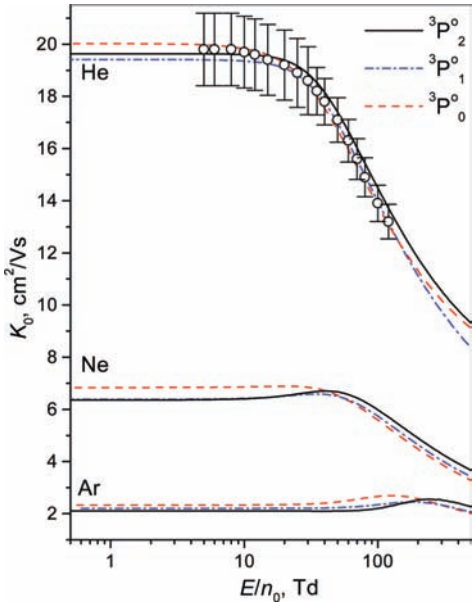

Figure 2. Comparison of calculated and experimental mobilities of Br^+ in RG = He, Ne, and Ar at 300 K. The quantity E/n_0 is the ratio of the electrostatic field strength to the number density of the neutral gas and 1 Td = 10^{-21} V m^2. Experiment is represented by the smoothed values[6] with the error bars estimated by the experimenters.[66]

TABLE 5: Statistical Comparison of Calculated and Smoothed Experimental Mobilities[6] of Br^+ in He at 300 K[a]

				$Br^+(^3P_2°)$		$Br^+(^3P_1°)$		$Br^+(^3P_0°)$	
E/n_0, Td	N	% expt	% calc	δ	χ	δ	χ	δ	χ
5−30	9	7.0	0.1	−0.02	0.13	0.18	0.21	−0.06	0.10
				−0.01	0.13	0.19	0.22	−0.05	0.09
30−120	8	5.0	0.1	−0.53	0.56	0.03	0.08	0.28	0.30
				−0.52	0.55	0.04	0.09	0.29	0.31

[a] Here N is the number of data points considered, % expt is the cited percentage experimental error, % calc is the convergence tolerance used in the calculations, and $^3P_J°$ refers to the state used in the calculations. The range of E/n_0 considered is specified in the corresponding column. The first line corresponds to the ^{79}Br isotope and the second to the ^{81}Br isotope. Neither the isotope nor the state was specified in ref 6.

They were then combined into the cross sections that refer to three individual states of Br^+: $^3P_2°$, $^3P_1°$, and $^3P_0°$. Specifically, we used the (W_1:W_2:W_3:W_4:W_5:W_6) weightings of the V_{X^+2},V_{I^+1},V_{I^+0},V_{II^+1},V_{II^+0}, and V_{III^+0} molecular states as follows: (2:2:1:0:0:0) for $^3P_2°$, (0:0:0:2:1:0) for $^3P_1°$, and (0:0:0:0:0:1) for $^3P_0°$.

The total transport cross sections were then used by program GC[95] to calculate the transport coefficients of Br^+ ions in RG; the ab initio mobilities were converged to within 0.1%. We obtained results for all three individual states of $^{79}Br^+$ and $^{81}Br^+$ isotopic ions moving through a naturally occurring mixture of each of the three RG. We used gas temperatures of 100, 200, 300, 400, and 500 K for all Br^+−RG pairs and also 4.35 and 82 K for Br^+−He. All of these results have been entered into the gaseous ion transport database[96] maintained at Chatham University.

Figure 2 shows a comparison of the calculated and experimental[6,66] mobilities for $^{79}Br^+$ in He at 300 K. A statistical comparison with the data is given in Table 5, where the dimensionless quantity δ is a measure of the relative difference compared to the combined experimental and calculational errors, while χ is a measure of the relative standard deviation compared to the sum of the squared error estimates. Values of $|\delta|$ that are substantially lower, alternatively higher, than 1 indicate that there is substantial agreement, alternatively disagreement, between the calculated and measured values, on average. Values of χ that are not much larger than $|\delta|$ indicate that there is little scatter in the experimental data and that the agreement between the calculated and measured values is uniform over all values of E/n_0, while values of χ substantially greater than $|\delta|$ indicate that at least one of these factors is not true.

Table 5 indicates that the calculated mobilities are virtually identical for $^{79}Br^+$ and $^{81}Br^+$. This is in agreement with first approximation results from kinetic theory,[91] which predicts that the gaseous ion mobility is inversely proportional to the square root of the reduced mass; i.e., the mobilities for $^{79}Br^+$ in He should exceed those for $^{81}Br^+$ in He by 0.06%.

Figure 2 and Table 5 indicate that, within the experimental error bars, it is not possible to determine which of the three spin−orbit states was present in the experiments, and indeed it is possible that a mixture was present (the experimentalists did not specify this, and were likely unable to determine it). This is based on the fact that none of the results differ by statistically significant amounts. However, based upon our results with Ne^+ in He,[92] it is probable that the ground J = 2 spin−orbit state was the one observed in experiments.

The values near E/n_0 = 0 are close to being constant because the average collision energies are essentially thermal. As E/n_0 increases, the mobilities in He decrease because even thermal energy is large enough, compared to the potential energy minimum, for collisions to probe the repulsive wall, so increases in energy due to increased E/n_0 just probe further up the wall. The mobility maxima for Ne and Ar occur at values of E/n_0 where the total (field plus thermal) average energy of the ion−neutral collisions is approximately equal to the minimum energy of the interaction potential. Beyond each maximum, the mobilities steadily decrease as the collisions probe further up on the potential wall. Between the low E/n_0 values and the mobility maxima, a small mobility minimum is found for Ar at 300 K; this was observed previously for Cd^+ and Hg^+,[97] for Zn^+,[98] for the coinage metals,[95] and for O^+,[99] and occurs in open-shell systems because the R^{-6} component of the long-range interaction is large. That the minimum occurs for Br^+ and not for Br^- is explained by the larger repulsion term in the latter case, which compensates for the attractive R^{-6} term; the importance of both attractive and repulsive effects for mobility minima is discussed in ref 95.

Figure 3 provides a direct comparison of the mobilities of Br^+ in He at 4.35 K with those of Br^- in He calculated with the CBS ab initio potential from ref 64. It shows that the different ions are indeed approaching the same mobility limit, determined by the dipole polarizability of He atom, as both T and E/n_0 tend to zero. The residual differences at E/n_0 = 0 reflect the influence of higher-order polarization interactions still not negligible at finite temperature. The Br^- mobility has a maximum at smaller E/n_0 and that is larger than the one for Br^+; both facts are consistent with the lower binding energy for the Br^-−He complex. As in the case of the cations, the $^{79}Br^-$ and $^{81}Br^-$ mobilities are essentially indistinguishable. Finally, the Br^+ mobilities exhibit a shallow minimum whereas the Br^- mobilities do not, as noted above.

ZEKE Spectroscopy. Photoionization spectroscopy of the neutral Br−RG complexes, using the zero electron kinetic energy variant, complement transport and scattering experiments by probing bound states of both neutral and cation systems, just as anion ZEKE photoelectron spectroscopy does for the

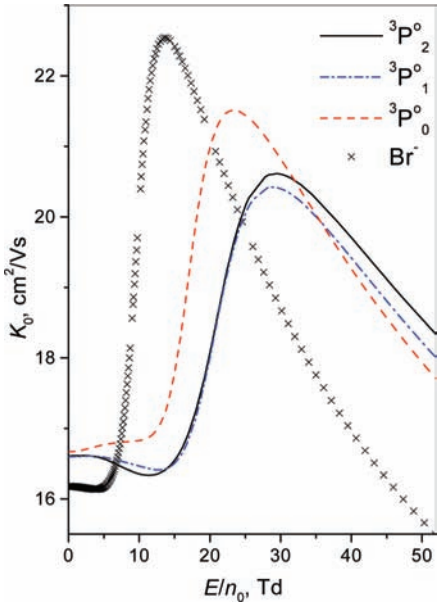

Figure 3. Comparison of the calculated mobilities of Br^- and Br^+ in He at 4.35 K.

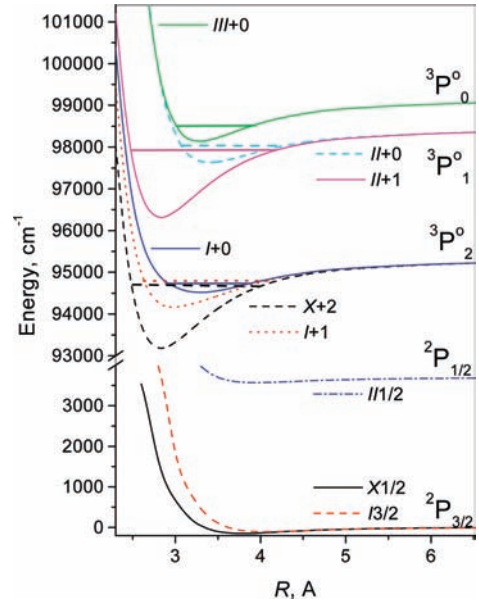

Figure 4. SO-coupled potential energy curves of the neutral and cation Br−Ar complexes. Horizontal lines indicate the predicted positions of the photoionization band maxima, as seen in Figure Figure 5 and Table 6.

anion and neutral ones.[21−26] To gain insight into this process, we present here simulations of the Br−Ar ZEKE spectra.

From the viewpoint of electronic structure, the $Br^+(^3P^\circ)-RG + e^- \leftarrow Br(^2P)-RG + h\nu$ process is similar to that involving the valence-isoelectronic species of oxygen anions and atoms, $O(^3P)-RG + e^- \leftarrow O^-(^2P)-RG + h\nu$. These systems have been studied employing ZEKE photoelectron spectroscopy, and the requisite theory for spectral simulations has been developed and applied (see, e.g., refs 100 and 101). In the present simulations, we made additional approximations by assuming a purely Franck−Condon excitation process and neglecting the rotational structure. We describe the SO-coupled X1/2, I3/2, and II1/2 states of the Br−Ar neutral using the CBS potentials and the atoms-in-molecule model parametrized by the measured SO splitting, $\Delta = 3685.2$ cm^{-1}, as described in ref 64. It is essential that equivalent theoretical descriptions of the initial and final states be achieved, and we thus use the results of Table 4 of the present work and the Table IV of ref 64 (ASO entry for Br−Ar therein) to obtain the required energy differences. The ionization energy for bromine ($^3P_2^\circ \leftarrow {}^2P_{3/2}$ transition) was taken as 95284.8 cm^{-1}.[83]

Figure 4 shows the potential energy curves of the states involved in the photoionization transitions, whereas Figure 5 presents an overview of the photoionization spectra in stick form. Each stick represents a particular vibronic transition from the ground, $v = 0$, vibrational levels of the three neutral electronic states to the vibrational energy levels, v^+, of the six cationic electronic states; the abscissa is on the electron binding energy (eBE) scale. Each spectrum consists of three features separated according to the SO splittings of the cation. The first of the three bands corresponds to the X^+2, I^+1, and I^+0 cation states, the two II^+0 and II^+1 bands form the second, and III^+0 forms the third. Owing to the small splitting between the X1/2 and I3/2 electronic states of the neutral (Figure 4), which both correlate to the lowest $Br^+(^2P_{3/2}) + Ar$ asymptote, the bands in the top two spectra can be seen practically to coincide. In contrast, the upper II1/2 state of the neutral is shifted toward lower eBE by approximately the SO splitting, Δ, that closely matches the cation splitting, Δ_0.

The difference between the very shallow neutral and relatively deep cation potentials leads to bands with a symmetric structure,

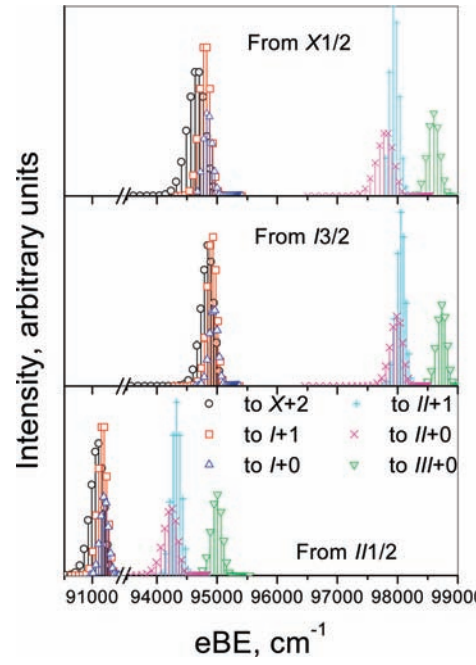

Figure 5. Stick spectrum corresponding to the vibrationally resolved photoionization of the Br−Ar($v = 0$) complex in its three lowest electronic states.

centered at the cation vibrational excitation $v_{center}{}^+$. In Table 6 we present the positions of $v^+ = 0 \leftarrow v = 0$ band origins and $v^+ \leftarrow v = 0$ band maxima estimated from the Franck−Condon envelopes. The positions of $v_{center}{}^+$ are also indicated in Figure 4 by horizontal lines in the corresponding potential energy curves.

In order to present the band structure in a more realistic way, a vibrationally resolved ZEKE spectrum in the 94200−94400 cm^{-1} region was simulated. This corresponds to the X^+2, I^+1, $I^+0 \leftarrow$ X1/2 ionizations. We have assumed a Gaussian line shape with fwhm = 5 cm^{-1}, a value typical for such ZEKE measurements. Figure 6 shows this spectrum simulated at two vibrational temperatures, 10 and 70 K. The lower temperature spectrum

TABLE 6: Origins and Maxima of the Bands in the Br−Ar Photoionization Spectrum (cm^{-1})[a]

	origin		maximum	
band	v^+	eBE	$v_{center}{}^+$	eBE
$X^+2 \leftarrow X$	0	93367	13, 14	94672
$I^+1 \leftarrow X$	0	94333	7, 8	94803
$I^+0 \leftarrow X$	0	94676	3	94827
$II^+0 \leftarrow X$	0	96503	13, 14	97809
$II^+1 \leftarrow X$	0	97796	2	97925
$III^+0 \leftarrow X$	0	98309	4	98600
$X^+2 \leftarrow I$	0	93328	17	94848
$I^+1 \leftarrow I$	0	94294	11	94934
$I^+0 \leftarrow I$	0	94637	7	94962
$II^+0 \leftarrow I$	0	96464	17	97984
$II^+1 \leftarrow I$	0	97756	5	98052
$III^+0 \leftarrow I$	0	98270	7	98734
$X^+2 \leftarrow II$	0	89657	17	91120
$I^+1 \leftarrow II$	0	90622	11	91193
$I^+0 \leftarrow II$	0	90965	7	91207
$II^+0 \leftarrow II$	0	92793	17	94256
$II^+1 \leftarrow II$	0	94084	5	94329
$III^+0 \leftarrow II$	0	94599	7	95009

[a] Initial vibrational excitation of the neutral is $v = 0$.

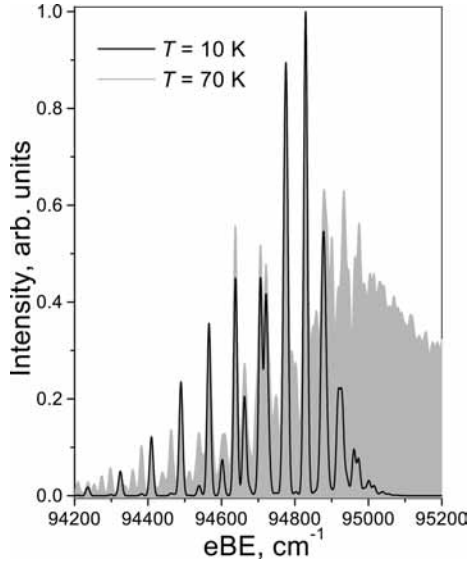

Figure 6. ZEKE spectrum of the Br−Ar complex in the region of the $X^+2 \leftarrow X1/2$, $v = 0$ band simulated at vibrational temperatures 10 and 70 K.

consists of three contributions, each originating from the X1/2,$v = 0$ level of the neutral and terminating at the three lowest states of the cation. Note that near the maximum, contributions from three cationic states overlap within the assumed resolution (see Figure 5). At the higher temperature, the structure becomes more complicated owing to the appearance of vibrational hot bands and also because of features associated with the I3/2 state of the neutral. Of note is that, despite the origin of the higher temperature spectrum being shifted toward lower eBE, its maximum appears at higher eBE. The simulations indicate that at 70 K well-resolved features are only likely to be observed on the low eBE side of the band. Indeed, the quasi-continuous structure evident in the 70 K spectrum occurs despite the fact that the simulations did not consider rotational broadening and assumed a reasonably high spectral resolution. As noted above, the clearest spectra are therefore expected at quite low vibrational temperatures and when the Br−Ar is formed in its lowest SO state. In a free jet expansion/molecular beam environment, Br will have to be formed in situ (for example via photolysis) and then coexpanded with Ar. It ought then to be possible to adjust the cooling to get cold rotational, vibrational, and spin−orbit distributions.

Summary

We have performed high-level ab initio scalar-relativistic calculations on the interaction potentials between $Br^+(^3P°)$ cation and rare gas atoms from He to Ar. The resulting potentials are comparable in accuracy with those of negatively charged $Br^-(^1S)$ and neutral $Br(^2P)$ analogues calculated before using the same ab initio approaches.[64]

Vectorial spin−orbit coupling was analyzed for the $Br^+(^3P_J°)$ multiplet. It was concluded that strong interactions with excited multiplets are difficult to treat within the state-interacting SO calculations for these complexes. Instead, the SO-coupled potentials of the Br^+−RG systems were obtained using the atoms-in-molecule model parametrized by the measured SO splittings. These potentials were used to derive the spectroscopic constants.

The mobilities of $Br^+(^3P_J°)$ cations in rare gases were computed for wide ranges of electric field strength and temperature. The differences in the calculated values for $^{79}Br^+$ and $^{81}Br^+$ were negligible. The present calculations on Br^+ agreed, within experimental and calculational errors, with available data in He at 300 K, although the latter are not sufficiently accurate to determine the distributions of the $^3P_J°$ states. We think that it is the $J = 2$ state present in the experiment based upon our previous work on Ne^+ in He.[92] The calculated mobilities for Br^+ in He at 4.35 K approach the polarization limit at low E/n_0, as do the mobilities for Br^- in He at the same temperature.

Combining the present Br^+−Ar potentials with those obtained previously for Br−Ar,[64] we have predicted ZEKE photoionization spectra in the region of $^3P° \leftarrow {}^2P$ ionization (90000−99000 cm^{-1}). The coarse-grained structure was determined by three features arranged in accord with the SO-splitting of the cation multiplet. Each feature consisted of the bands that correspond to molecular states correlating to the particular fine-structure J-state. Band overlapping resulted from the large difference in the shapes of neutral and cation potentials that shifts the band maxima toward high energy from the origin. Spectral simulations revealed the complex structure of the features and the strong dependence of the ZEKE spectra on temperature.

Acknowledgment. The work of L.A.V. was supported by the National Science Foundation under Grant CHE-0718024. T.G.W. and E.P.F.L. are grateful for computing time at the NSCCS, funded by the EPSRC (U.K.). A.A.B. is thankful for the support from the Russian Basic Research Fund under the project 09-03-92425-KE.

References and Notes

(1) Hirschfelder, J. O.; Curtiss, C. F.; Bird, R. B. *Molecular Theory of Gases and Liquids*; Wiley: New York, 1954.
(2) Aquilanti, V.; Grossi, G. *J. Chem. Phys.* **1980**, *73*, 1165.
(3) Ellis, H. W.; Pai, R. Y.; McDaniel, E. W.; Mason, E. A.; Viehland, L. A. *At. Data Nucl. Data Tables* **1976**, *17*, 177.
(4) Ellis, H. W.; McDaniel, E. W.; Albritton, D. L.; Viehland, L. A.; Lin, S. L.; Mason, E. A. *At. Data Nucl. Data Tables* **1978**, *22*, 179.
(5) Ellis, H. W.; Thackston, M. G.; McDaniel, E. W.; Mason, E. A. *At. Data Nucl. Data Tables* **1984**, *31*, 113.
(6) Viehland, L. A.; Mason, E. A. *At. Data Nucl. Data Tables* **1995**, *60*, 37.
(7) Lozeille, J.; Winata, E.; Viehland, L. A.; Soldán, P.; Lee, E. P. F.; Wright, T. G. *Phys. Chem. Chem. Phys.* **2002**, *4*, 3601.
(8) Lozeille, J.; Winata, E.; Viehland, L. A.; Soldán, P.; Lee, E. P. F.; Wright, T. G. *J. Chem. Phys.* **2003**, *119*, 3729.

(9) Viehland, L. A.; Lozeille, J.; Soldán, P.; Lee, E. P. F.; Wright, T. G. *J. Chem. Phys.* **2004**, *121*, 341.
(10) Hickling, H. L.; Viehland, L. A.; Shepherd, D. T.; Soldán, P.; Lee, E. P. F.; Wright, T. G. *Phys. Chem. Chem. Phys.* **2004**, *6*, 4233.
(11) Kirkpatrick, C. C.; Viehland, L. A. *Chem. Phys.* **1985**, *98*, 221.
(12) Viehland, L. A.; Kirkpatrick, C. C. *Chem. Phys.* **1996**, *202*, 285.
(13) Koutselos, A. D.; Mason, E. A.; Viehland, L. A. *J. Chem. Phys.* **1990**, *93*, 7125.
(14) Mansky, E. J.; Flannery, M. R. *J. Chem. Phys.* **1993**, *99*, 1962. **1994**, *100*, 5391 (Erratum).
(15) Ahlrichs, R.; Böhm, H. J.; Brode, S.; Tang, K. T.; Toennies, J. P. *J. Chem. Phys.* **1988**, *88*, 6290.
(16) Wilson, W.; Heinbockel, J. H.; Outlaw, R. A. *J. Chem. Phys.* **1988**, *89*, 929.
(17) Patil, S. H. *J. Chem. Phys.* **1988**, *89*, 6357.
(18) Waldman, M.; Gordon, R. G. *J. Chem. Phys.* **1979**, *71*, 1325.
(19) Cappelletti, D.; Liuti, G.; Pirani, F. *Chem. Phys. Lett.* **1991**, *183*, 297.
(20) Aquilanti, V.; Cappelletti, D.; Pirani, F. *Chem. Phys.* **1996**, *209*, 299.
(21) Zhao, Y.; Yourshaw, I.; Reiser, G.; Arnold, C. C.; Neumark, D. M. *J. Chem. Phys.* **1994**, *101*, 6538.
(22) Yourshaw, I.; Zhao, Y.; Neumark, D. M. *J. Chem. Phys.* **1996**, *105*, 351.
(23) Yourshaw, I.; Lenzer, T.; Reiser, G.; Neumark, D. M. *J. Chem. Phys.* **1998**, *109*, 5247.
(24) Lenzer, T.; Furlanetto, M. R.; Asmis, K. R.; Neumark, D. M. *J. Chem. Phys.* **1998**, *109*, 10754.
(25) Lenzer, T.; Furlanetto, M. R.; Pivonka, N. L.; Neumark, D. M. *J. Chem. Phys.* **1999**, *110*, 6714.
(26) Lenzer, T.; Yourshaw, I.; Furlanetto, M. R.; Reiser, G.; Neumark, D. M. *J. Chem. Phys.* **1999**, *110*, 9578.
(27) Buchachenko, A. A.; Krems, R. V.; Szczęśniak, M. M.; Xiao, Y.-D.; Viehland, L. A.; Chałasiński, G. *J. Chem. Phys.* **2001**, *114*, 9919.
(28) Buchachenko, A. A.; Szczęśniak, M. M.; Chałasiński, G. *J. Chem. Phys.* **2001**, *114*, 9929.
(29) Buchachenko, A. A.; Tscherbul, T. V.; Kłos, J.; Szczęśniak, M. M.; Chałasiński, G.; Webb, R.; Viehland, L. A. *J. Chem. Phys.* **2005**, *122*, 194311.
(30) Buchachenko, A. A.; Kłos, J.; Szczęśniak, M. M.; Chałasiński, G.; Wright, T. G.; Wood, E. L.; Viehland, L. A.; Qing, E. *J. Chem. Phys.* **2006**, *125*, 064305.
(31) Kuznetsova, L. A.; Kuzyakov, Y. Y.; Shpanskii, V. A.; Khutoretskii, V. M. *Vestn. Mosk. Univ., Ser. 2: Khim.* **1964**, *19*, 19.
(32) Golde, M. F.; Thrush, B. A. *Chem. Phys. Lett.* **1974**, *29*, 486.
(33) Velasco, J. E.; Setser, D. W. *J. Chem. Phys.* **1975**, *62*, 1990.
(34) Searles, S. K.; Hart, G. A. *Appl. Phys. Lett.* **1975**, *27*, 243.
(35) Ewing, J. J.; Brau, C. A. *Appl. Phys. Lett.* **1975**, *27*, 350.
(36) Magano, J. A.; Jacob, J. H. *Appl. Phys. Lett.* **1975**, *27*, 495.
(37) Clevenger, J. O.; Tellighuisen, J. *J. Chem. Phys.* **1995**, *103*, 9611.
(38) Becker, C. H.; Casavecchia, P.; Lee, Y. T. *J. Chem. Phys.* **1978**, *69*, 2377.
(39) Becker, C. H.; Valentini, J. J.; Casavecchia, P.; Sibener, S. J.; Lee, Y. T. *Chem. Phys. Lett.* **1979**, *61*, 1.
(40) Becker, C. H.; Casavecchia, P.; Lee, Y. T. *J. Chem. Phys.* **1979**, *70*, 2986.
(41) Casavecchia, P.; He, G.; Sparks, R. K.; Lee, Y. T. *J. Chem. Phys.* **1981**, *75*, 710.
(42) Aquilanti, V.; Luzzatti, E.; Pirani, F.; Volpi, G. G. *J. Chem. Phys.* **1988**, *89*, 6165.
(43) Aquilanti, V.; Cappelletti, D.; Lorent, V.; Luzzatti, E.; Pirani, F. *Chem. Phys. Lett.* **1992**, *192*, 153.
(44) Aquilanti, V.; Cappelletti, D.; Lorent, V.; Luzzatti, E.; Pirani, F. *J. Phys. Chem.* **1993**, *97*, 2063.
(45) Hwang, C.-J.; Jiang, R.-C.; Su, T.-M. *J. Chem. Phys.* **1986**, *84*, 5095.
(46) Hwang, C.-J.; Jiang, R.-C.; Su, T.-M. *J. Chem. Phys.* **1989**, *91*, 1626.
(47) Fletcher, I. S.; Husain, D. *Faraday Trans., Chem. Soc. 2* **1978**, *74*, 203.
(48) Sotnichenko, S. A.; Bokun, V.Ch.; Nadkhin, A. I. *Chem. Phys. Lett.* **1988**, *153*, 560.
(49) Tyndall, G. S.; Orlando, J. J.; Kegley-Owen, C. S. *Faraday Trans., Chem. Soc.* **1995**, *91*, 3055.
(50) Johnson, J. O.; Perram, G. C.; Roh, W. B. *J. Chem. Phys.* **1996**, *104*, 7052.
(51) Chichinin, A. I. *J. Chem. Phys.* **2000**, *112*, 3772.
(52) Hay, P. J.; Dunning, T. H., Jr. *J. Chem. Phys.* **1977**, *66*, 1306.
(53) Hay, P. J.; Dunning, T. H., Jr. *J. Chem. Phys.* **1978**, *69*, 134.
(54) Hay, P. J.; Dunning, T. H., Jr. *J. Chem. Phys.* **1978**, *69*, 2209.
(55) Adams, G. F.; Chabalowski, C. F. *J. Phys. Chem.* **1994**, *98*, 5878.
(56) Burcl, R.; Cybulski, S. M.; Szczęśniak, M. M.; Chałasiński, G. *J. Chem. Phys.* **1995**, *103*, 299.
(57) Naumkin, F. Y.; McCourt, F. R. W. *Chem. Phys. Lett.* **1998**, *294*, 71.
(58) Burcl, R.; Krems, R. V.; Buchachenko, A. A.; Szczęśniak, M. M.; Chałasiński, G.; Cybulski, S. M. *J. Chem. Phys.* **1998**, *109*, 2144.
(59) Naumkin, F. Y. *ChemPhysChem* **2001**, *2*, 121.
(60) Partridge, H.; Stallcop, J. R.; Levin, E. *J. Chem. Phys.* **2001**, *115*, 6471.
(61) de Lara-Castells, M. P.; Krems, R. V.; Buchachenko, A. A.; Delgado-Barrio, G.; Villarreal, P. *J. Chem. Phys.* **2001**, *115*, 10438.
(62) Léonard, C.; Le Quéré, F.; Peterson, K. *Phys. Chem. Chem. Phys.* **2005**, *7*, 1694.
(63) Gray, R. B.; Wright, T. G.; Wood, E. L.; Viehland, L. A. *Phys. Chem. Chem. Phys.* **2006**, *8*, 4752.
(64) Buchachenko, A. A.; Grinev, T. A.; Wright, T. G.; Viehland, L. A. *J. Chem. Phys.* **2008**, *128*, 064317.
(65) Twiddy, N. D. Personal communications, 1983.
(66) Hamdan, M.; Birkinshaw, K. *Int. J. Mass Spectrom. Ion Processes* **1986**, *70*, 221.
(67) Werner, H.-J.; Knowles, P. J.; Lindh, R.; Manby, F. R.; Schütz, M.; et al. *MOLPRO, version 2008.1, a package of ab initio programs*, 2008.
(68) Peterson, K. A.; Figgen, D.; Goll, E.; Stoll, H.; Dolg, M. *J. Chem. Phys.* **2003**, *119*, 11113.
(69) Dunning, T. H., Jr. *J. Chem. Phys.* **1989**, *90*, 1007.
(70) Woon, D. E.; Dunning, T. H., Jr. *J. Chem. Phys.* **1993**, *93*, 1358.
(71) Boys, S. F.; Bernardi, F. *Mol. Phys.* **1970**, *19*, 553.
(72) Halkier, A.; Helgaker, T.; Jørgensen, P.; Klopper, W.; Koch, H.; Olsen, J.; Wilson, A. K. *Chem. Phys. Lett.* **1998**, *286*, 243.
(73) Halkier, A.; Helgaker, T.; Jørgensen, P.; Klopper, W.; Olsen, J. *Chem. Phys. Lett.* **1999**, *302*, 437.
(74) Coker, H. *J. Phys. Chem.* **1976**, *80*, 2078.
(75) Kutzner, M.; Felton, M.; Winn, D. *Phys. Rev. A* **1992**, *45*, 7761.
(76) Hättig, C.; Heβ, B. A. *J. Chem. Phys.* **1998**, *108*, 3863.
(77) Medve, M.; Fowler, P. W.; Hutson, J. M. *Mol. Phys.* **2000**, *98*, 453.
(78) Fleig, T.; Sadlej, A. J. *Phys. Rev. A* **2002**, *65*, 032506.
(79) Angel, J. R. P.; Sandaras, P. G. H. *Proc. R. Soc.London, Ser. A* **1968**, *305*, 125.
(80) Aquilanti, V.; Liuti, G.; Pirani, F.; Vecchiocattivi, F. *J. Chem. Soc., Faraday Trans. 2* **1989**, *85*, 955.
(81) Cambi, R.; Cappelletti, D.; Liuti, G.; Pirani, F. *J. Chem. Phys.* **1991**, *95*, 1852.
(82) Cappelletti, D.; Liuti, G.; Pirani, F. *Chem. Phys. Lett.* **1991**, *183*, 297.
(83) Ralchenko, Yu.; Jou, F.-C.; Kellener, D. E.; Kamida, A. E.; Musgrove, A.; Reader, J.; Wiese, W. L.; Olsen, K. *NIST Atomic Database*; NIST: Gaithersburg, MD, 2007 (http://physics.nist.gov/PhysRefData/).
(84) Dolg, M.; Stoll, H.; Flad, H.-J.; Preuss, H. *J. Chem. Phys.* **1992**, *97*, 1162.
(85) Berning, A.; Schweizer, M.; Werner, H.-J.; Knowles, P. J.; Palmieri, P. *Mol. Phys.* **2003**, *98*, 1823.
(86) Balasubramanian, K.; Kaufman, J. J.; Hariharan, P. C.; Koski, W. S. *Chem. Phys. Lett.* **1986**, *129*, 165.
(87) Ma, Z.; Liu, K.; Harding, L. B.; Komotos, M.; Schatz, G. C. *J. Chem. Phys.* **1994**, *100*, 8026.
(88) Krems, R. V.; Buchachenko, A. A. *J. Phys. B* **2000**, *33*, 4551.
(89) Aquilanti, V.; Luzzatti, E.; Pirani, F.; Volpi, G. G. *J. Chem. Phys.* **1980**, *73*, 118.
(90) Aquilanti, V.; Vecchiocattivi, F. *Chem. Phys. Lett.* **1989**, *156*, 109.
(91) Mason E. A. McDaniel, E. W. *Transport Properties of Ions in Gases*; Wiley: New York, 1988.
(92) Wright, T. G.; Gray, B. R.; Viehland, L. A.; Johnsen, R. *J. Chem. Phys.* **2008**, 184307.
(93) Viehland, L. A. *Comput. Phys. Commun.* **2001**, *142*, 7.
(94) Viehland, L. A. *Chem. Phys.* **1982**, *70*, 149.
(95) Yousef, A.; Shrestha, S.; Viehland, L. A.; Lee, E. P. F.; Gray, B. R.; Ayles, V. L.; Wright, T. G.; Breckenridge, W. H. *J. Chem. Phys.* **2007**, *127*, 154309.
(96) A username and password for accessing this database will be supplied upon request to viehland@chatham.edu.
(97) Qing, E.; Viehland, L. A.; Lee, E. P. F.; Wright, T. G. *J. Chem. Phys.* **2006**, *124*, 044316.
(98) Lee, E. P. F.; Gray, B. R.; Joyner, N. A.; Johnson, S. H.; Viehland, L. A.; Breckenridge, W. H.; Wright, T. G. *Chem. Phys. Lett.* **2007**, *450*, 19.
(99) Danailov, D. M.; Viehland, L. A.; Johnsen, R.; Wright, T. G.; Dickinson, A. D. *J. Chem. Phys.* **2008**, *128*, 134302.
(100) Buchachenko, A. A.; Jakowski, J.; Chałasiński, G.; Szczęśniak, M. M.; Cybulski, S. M. *J. Chem. Phys.* **2000**, *112*, 5852.
(101) Garand, E.; Buchachenko, A. A.; Yacovitch, T. I.; Szczęśniak, M. M.; Chałasiński, G.; Neumark, D. M. *J. Phys. Chem. A*, In this issue DOI: 10.1021/jp903819m.

JP903811B